

Some Properties of Dust Outside the Galactic Disk

G. A. Gontcharov*

January 5, 2018

Pulkovo Astronomical Observatory, Russian Academy of Sciences, Pulkovskoe sh. 65, St. Petersburg, 196140 Russia

Key words: interstellar dust grains; color-magnitude diagrams, giant and subgiant stars

The joint use of accurate near- and mid-infrared photometry from the 2MASS and WISE catalogues has allowed the variations of the extinction law and the dust grain size distribution in high Galactic latitudes ($|b| > 50^\circ$) at distances up to 3 kpc from the Galactic midplane to be analyzed. The modified method of extrapolation of the extinction law applied to clump giants has turned out to be efficient for separating the spatial variations of the sample composition, metallicity, reddening, and properties of the medium. The detected spatial variations of the coefficients $E_{(H-W1)}/E_{(H-Ks)}$, $E_{(H-W2)}/E_{(H-Ks)}$, and $E_{(H-W3)}/E_{(H-Ks)}$ are similar for all high latitudes and depend only on the distance from the Galactic midplane. The ratio of short-wavelength extinction to long-wavelength one everywhere outside the Galactic disk has been found to be smaller than that in the disk and, accordingly, the mean dust grain size is larger, while the grain size distribution in the range 0.5 – 11 microns is shifted toward coarse dust. Specifically, the mean grain size initially increases sharply with distance from the Galactic midplane, then decreases gradually, approaching a value typical of the disk at $|Z| \approx 2.4$ kpc, and, further out, stabilizes or may increase again. The coefficients under consideration change with coordinate Z with a period of about 1312 ± 40 pc, coinciding every 656 ± 20 pc to the south and the north and showing a significant anticorrelation between their values

*E-mail: georgegontcharov@yahoo.com

in the southern and northern hemispheres at intermediate Z . Thus, there exists a unified large-scale periodic structure of the interstellar medium at high latitudes within at least 5 kpc. The same periodic variations have also been found for the extinction coefficient R_V within 600 pc of the Galactic midplane through the reduction of different photometric data for stars of different classes.

INTRODUCTION

The wavelength dependence of interstellar extinction (extinction law) is related primarily to the dust grain size distribution in the absorbing medium. In the most widespread media, the extinction maximum in a region of space occurs at a wavelength that coincides in order of magnitude with the mean dust grain diameter in this region (Bochkarev 2010). For example, the commonly considered extinction A_V in the photometric V band with a wavelength of 0.55 microns and, in general, the visual extinction is produced predominantly by submicron sized dust grains, whereas the infrared (IR) one is produced by supermicron ones. Conclusions about the physical properties of dust in the region of space under consideration and about the contribution of dust to the total mass of the matter can be reached by studying the wavelength dependence of extinction. Conversely, the extinction can be calculated by studying the properties of the dust medium.

Numerous studies of the dust and extinction in the Galactic disk, including those in the solar neighborhood, have shown that submicron dust grains producing an essentially selective extinction, i.e., one that decreases appreciably with increasing wavelength in such a way that the IR extinction is insignificant compared to the visual one, dominate here.

The dust and extinction in regions of the Galaxy far from the Sun at its high latitudes outside the disk have been studied more poorly. Clearly, the extinction here is low. However, the ratio of visual to IR extinction and, accordingly, the content of large dust grains in the interstellar medium is still difficult to estimate here.

IR photometry of stars in a small region of space or a small number of stars is useless for these estimations, because some of the stars of various classes exhibit an unpredictable IR emission. Only averaging the data for many stars in regions of space that definitely exceed the typical size of an interstellar cloud (> 10 pc) allows its influence to be smoothed out.

Only the accurate multicolor broadband IR photometry for millions of stars over the entire sky from the 2MASS and WISE catalogues obtained in recent years allows the coarse dust and IR extinction outside the Galactic disk to be investigated for the first time. The 2MASS (2-Micron All-Sky Survey) catalogue (Skrutskie et al. 2006) was produced in 2006 as a result of ground-based observations in 1997-2001 and contains photometry for more than 400 million stars over the entire sky in the near-IR J (1.23 microns), H (1.64 microns), and K_s (2.15 microns) bands. The WISE catalogue (Wright

et al. 2010) was produced in 2012 as a result of the observations performed in 2010 with the Wide-field Infrared Survey Explorer space telescope and contains photometry for more than 500 million stars over the entire sky, including almost all 2MASS stars, in the mid-IR *W1* (3.3 microns), *W2* (4.6 microns), *W3* (11 microns), and *W4* (22 microns) bands.

IR surveys of selected sky regions, for example, the mid-IR survey of the region toward the Galactic center with the IRAC camera of the Spitzer space telescope, have also been made in recent years. The data from this survey used together with the 2MASS data allowed Zasowski et al. (2009) to detect largescale systematic spatial variations of the extinction law and, consequently, the sizes and other properties of dust grains in the inner (relative to the Sun) Galactic disk within 15 kpc. Supermicron- and submicron-sized dust apparently dominates in the parts of the disk close to the Galactic center and in the solar neighborhood, respectively. These variations have such a large scale that they are actually characteristic of a diffuse medium rather than small dense clouds and star-forming regions.

Gontcharov (2013) tested the results by Zasowski et al. (2009) in the first and fourth Galactic quadrants of the disk using WISE data instead of Spitzer ones and carried out a similar search for the spatial variations of dust properties in the second and third Galactic quadrants, where only the 2MASS and WISE data are available. The result by Zasowski et al. (2009) was confirmed for the inner (relative to the Sun) Galactic disk: the mean dust grain size decreases with increasing Galactocentric distance. However, in the outer Galactic disk that was not considered by Zasowski et al. (2009), this trend is reversed: the dust grains at the disk edge are, on average, larger than those in the solar neighborhood. These variations refer to the region with a radius of more than 5 kpc around the Sun.

When analyzing the extinction law and dust properties in certain directions at latitudes $|b| = 10^\circ$, Gontcharov (2013) found the mean dust grain size to increase with distance from the Galactic midplane.

This confirms the previous result by Gontcharov (2012a) presented in the three-dimensional map of variations in extinction coefficient $R_V \equiv A_V/E_{(B-V)}$ within 600 pc of the Sun. This map was obtained using visual photometry from the Tycho-2 catalogue (Høg et al. 2000) and 2MASS IR photometry. According to this map, R_V changes systematically with distance from the Galactic midplane. It has a sharp minimum in the layer with a thickness of less than 200 pc near the midplane, increases with distance from the midplane, reaching its maximum at distances $|Z| \approx 150 \div 400$ pc

from the midplane, and slightly decreases at $|Z| \approx 500$ pc. Figure 1 shows the detected variations of R_V with heliocentric distance for the region with a radius of 8° around the Galactic north (black diamonds, curve, and vertical error bars) and south (grey squares, curve, and vertical error bars) poles. This figure can be compared with Fig. 6 from Gontcharov (2012a). The coefficient R_V is seen to have a classical value of 3.1 near the Sun. In addition, the changes of R_V to the south and the north anticorrelate at $|Z| > 100$ pc: the increase to the north of the equator corresponds to the decrease at the same distance to the south and vice versa. This anticorrelation is discussed below.

The large-scale general Galactic trends in the variations of dust properties can be explained by the influence of the spiral pattern as probably the only place where the dust is fragmented and sorted by size. As a result, as Gontcharov (2013) assumed, fine dust exists only in the part of the Galactic disk where the spiral pattern operates, i.e., far from both the Galactic center and the edge. The fraction of fine dust at the Galactic center, at the disk edge, and outside the disk should then be minimal. This study is devoted to testing this assumption regarding the Galactic regions outside the disk. For the convenience of comparing the results, the applied method and the quantities considered here are analogous to those in Zasowski et al. (2009) and Gontcharov (2013).

DATA REDUCTION

For this study, we selected stars at high latitudes ($|b| > 50^\circ$) common to 2MASS and WISE with an accuracy of their photometry in the J , H , K_s , $W1$, and $W2$ bands better than 0.05^m . In this case, the sample remains almost complete in the range of magnitudes $6^m < K_s < 14^m$.

Because of the unexpected loss of its coolant ahead of schedule, the WISE spacecraft reduced the observing period and did not achieve a high photometric accuracy in the $W3$ and $W4$ bands. Therefore, the results in these bands are barely considered here.

In this study, we have made an attempt to investigate the properties of dust outside the disk for the first time by using only IR photometry. This attempt is based on the advantages of jointly using near- (2MASS) and mid-IR (Spitzer or WISE) photometry to which attention was first drawn by Majewski et al. (2011). One of these advantages is the independence of the

$(H - W2)$ color index on stellar metallicity and age. These advantages are discussed in more detail below.

The high latitudes under consideration differ from the disk regions considered by Zasowski et al. (2009) and Gontcharov (2013) by a smaller number of stars, a smaller reddening/extinction, and a larger metallicity gradient. Allowance for these peculiarities forced us to slightly modify the method applied by Zasowski et al. (2009) and Gontcharov (2013). They, in turn, adapted the classical method of determining the spatial variations of the extinction law and dust properties, the method of extrapolation of the extinction law (Straizys 1977; Gontcharov 2012a), for the infrared. This method is commonly used in its classical form to determine the coefficient R_V from the formula $A_V/E_{(B-V)} \approx 1.1E_{(V-K)}/E_{(B-V)}$. The ratio of reddenings (color excesses) $E_{(V-K)}/E_{(B-V)}$ is a characteristic of the dust grain size distribution in the range from about 0.5 to 2 microns. The analogous coefficients $E_{(H-W1)}/E_{(H-Ks)}$, $E_{(H-W2)}/E_{(H-Ks)}$, and $E_{(H-W3)}/E_{(H-Ks)}$ considered here following Zasowski et al. (2009) and Gontcharov (2013) characterize the extinction law and the dust grain size distribution in the range from about 2 to 11 microns.

The method of extrapolation of the extinction law requires the following in the spatial cell under consideration: (1) a representative sample of stars with the same unreddened spectral energy distribution; (2) the reddening gradient within this cell should be larger than the photometric errors; and (3) to compare the reddenings at different wavelengths, at least one of the color indices used should redden noticeably within the cell, i.e., the reddening and extinction should be sufficiently large. When using only IR photometry, the reddening and extinction are so small that we have to consider spatial cells with a large number of stars and to watch carefully the balance of errors. In most of the space under consideration, we attempt to reveal effects at a 0.01^m level using photometry with a median accuracy of 0.02^m in each band for an individual star. Accordingly, the median accuracy of each color index used for an individual star is about 0.03^m . Therefore, we have to consider cells with tens and hundreds of stars. The task is complicated by the fact that high latitudes are poor in stars.

In such a situation, averaging the data for many stars in the cell makes sense only if their spectral energy distribution is the same and/or predictable with an accuracy better than 0.01^m depending on the known parameters. In practice, however, this distribution changes at least in one of the bands under consideration by more than 0.1^m for neighboring classes of stars (for example,

red giant branch (RGB) stars and clump giants) as well as with metallicity and reddening. As it turned out, only the age may not be considered: stars with ages older than 7×10^9 yr dominate at high latitudes and the spectral energy distribution within most of the classes at such an age changes with age within 0.01^m .

Thus, the method of extrapolation of the extinction law is efficient only for a large sample of highluminosity stars with a stable spectral energy distribution. Gontcharov (2012a) applied it for OB and RGB KIII stars. Consistent spatial variations of the coefficient R_V were found for so different classes. In this study, following Zasowski et al. (2009) and Gontcharov (2013), we applied this method to clump giants.

Clump giants are evolved stars with nuclear reactions in their helium cores. Their evolutionary status and characteristics were considered in detail by Gontcharov (2008) when analyzing a sample of 97 348 such stars from the Hipparcos (ESA 1997; van Leeuwen 2007) and Tycho-2 catalogues mostly within 1 kpc of the Sun. In particular, their empirical mean absolute magnitude $\overline{M_{K_s}} = -1.52^m$ obtained by Gontcharov (2008) by taking into account the Hipparcos parallaxes and used below is consistent, within 0.05^m , with the theoretical estimate from the Padova database of evolutionary tracks and isochrones (<http://stev.oapd.inaf.it/cmd>; Marigo et al. 2008; Bressan et al. 2012; here and below, all theoretical results of modeling the evolution of stars were taken from the Padova database) for the mixture of clump giants with metallicity \mathbf{Z} from 0.004 to 0.020 and a mass from 0.9 to $3 M_\odot$ (accordingly, an age up to 10×10^9 yr) at mean metallicity $\mathbf{Z} \approx 0.014$ (i.e., $Fe/H \approx -0.13$, slightly lower than the solar one) and a mass of 1.4 solar masses assumed in Tycho-2. Encompassing a larger space, the sample of clump giants considered here should have a wide range of metallicities, masses, and ages than the sample from Tycho-2. However, even the variations in age up to 14×10^9 yr and in \mathbf{Z} from 0.001 to 0.020, according to the Padova database, lead to variations in $\overline{M_{K_s}}$ within $\pm 0.1^m$, an insignificant dependence of $\overline{M_{K_s}}$ on color indices, and a small scatter of individual M_{K_s} around $\overline{M_{K_s}}$ ($\sigma(M_{K_s}) = 0.3^m$). This allows the distance r for each selected star to be calculated with an accuracy of 15%:

$$r = 10^{(K_s + 1.52 + 5)/5}. \quad (1)$$

The extinction A_{K_s} should have entered into this formula. However, its value and uncertainty at the latitudes under consideration ($|b| > 50^\circ$) are

small compared to the scatter of individual M_{Ks} : according to Gontcharov (2012b), $A_V < 0.3^m$; then, $A_{Ks} < 0.03^m$, given the most commonly used estimates of the extinction law, for example, from Cardelli et al. (1989), Draine (2003), and Indebetouw et al. (2005). Therefore, the extinction may be neglected in this formula for high latitudes.

The IR photometry is inaccurate not only for faint stars but also for the brightest ones ($Ks < 6^m$). Therefore, in the sample there are almost no clump giants within 400 pc of the Sun. However, the sample is almost complete in the range of distances from 0.4 to 3 kpc. All of the results presented below refer to this range of distances.

The selection of clump giants as all stars in one of the regions of enhanced star density on the $(J - Ks) - Ks$ diagram has been used many times, for example, by Lopez-Corredoira et al. (2002), Indebetouw et al. (2005), and Gontcharov (2013).

Figure 2 gives an example of the $(J - Ks) - Ks$ diagram for two of the sky regions under consideration: (a) with a radius of 8° around the Galactic north pole and (b) in the sky sector $-15^\circ < l < 15^\circ$, $-61^\circ < b < -53^\circ$, i.e., the regions, respectively, with the smallest and largest extinction among all those considered in this study. It can be seen from the figure that the reddening effect here is insignificant and the distributions of stars on the diagram in these regions barely differ. The left, central, and right clouds of stars consist mostly of O-F main-sequence stars, clump giants, and red dwarfs, respectively. The admixtures of subdwarfs, subgiants, supergiants, RGB stars, and other classes are small compared to the main categories. It can be seen that these three categories of stars barely mix at $Ks < 11^m$. This value has become one of the criteria for selecting a comparatively pure sample of clump giants, while the main criterion is

$$0.5^m < (J - Ks) < 0.76^m. \quad (2)$$

The selected stars are marked by the larger signs in the upper parts of the graphs. This criterion efficiently separates the clump giants from the stars with a different spectral energy distribution, which, among other things, manifests itself in different absolute magnitudes M_J and M_{Ks} . In this way, not only a high efficiency of the method but also a sufficient accuracy of the photometric distances obtained below from M_{Ks} is achieved. In addition to other stars, this criterion also rejects the overwhelming majority of subgiants and RGB stars with $(J - Ks) < 0.5^m$ and $(J - Ks) > 0.76^m$, respectively (in

the figure, leftward and rightward of the cloud of selected stars, respectively). However, even on the Hertzsprung- Russell diagram the red giant branch and the clump of giants are mixed. Therefore, of course, the subgiants and RGB stars cannot be completely excluded from our sample. It is only important that their admixture does not distort the average spectral energy distribution for the stars in each spatial cell under consideration. The theoretical data on the evolution of stars from the Padova database show that the admixture of subgiants and RGB stars for the range (2) at $Ks > 7^m$ accounts for no more than 30% of the sample and introduces distortions into the average spectral energy distribution for the subsamples of 200 stars considered below by no more than 0.01^m in each band under consideration. At $Ks < 7^m$ the influence of the admixture of RGB stars should theoretically be larger, because their luminosity is, on average, higher than that of clump giants. Below we detected this influence when analyzing the $Ks - (H - W2)$ diagrams at $Ks < 7^m$, i.e., according to Eq. (1), at $r < 500$ pc. The results of this study refer to $r > 500$ pc and, therefore, are not affected by the admixture of bright RGB stars.

For the range (2), as Gontcharov (2013) showed, the admixture of dwarfs outside the disk is more than 10%. However, contrary to the assumption made by Gontcharov (2013), this admixture can be revealed by using not only the reduced proper motions but also the $(H - W2)$ and $(Ks - W2)$ color indices, as was proposed by Majewski et al. (2011) and is realized below.

According to the evolutionary tracks and isochrones of stars from the Padova database, all the color indices of the clump giants considered here are almost independent of their age in the range $7 \times 10^9 - 14 \times 10^9$ yr but depend significantly on their metallicity. Therefore, in contrast to Zasowski et al. (2009) and Gontcharov (2013), who selected the clump giants in the disk, where the metallicity gradient is small, here we should apply a more sophisticated selection procedure.

Figure 3 shows the theoretical spectral energy distribution for a typical clump giant with an age of 10×10^9 yr for metallicities $\mathbf{Z} = 0.015$ (black squares and solid curve), $\mathbf{Z} = 0.006$ (grey diamonds and solid curve), and $\mathbf{Z} = 0.004$ (black circles and dashed line). in the (from left to right) J , H , Ks , $W1$, $W2$, $W3$, and $W4$ bands expressed in magnitudes relative to the $W2$ magnitude. These metallicities correspond to $Fe/H \approx -0.1, -0.5, -0.7$, i.e., according to present views, they reflect the transition from the nearly solar metallicity of the thin disk to a metallicity typical of the thick disk-halo

boundary. It can be seen that, as has been pointed out above, for such a wide range of metallicities the $(H - W2)$ color index changes by less than 0.01^m . Therefore, the systematic change in $(H - W2)$ should be attributed only to the change in sample composition and reddening.

The $(H - Ks)$ and $(Ks - W2)$ color indices also change only slightly with metallicity.

It should also be noted that this spectral energy distribution corresponds to blackbody radiation in the J , H , and Ks bands, slightly deviates from it in the $W1$ and $W2$ bands, and deviates significantly due to the emission in the $W3$ and $W4$ bands.

It is also important that the $(J - H)$ color index decreases with decreasing metallicity but is known to increase with increasing extinction. This allows the metallicity and extinction variations with distance from the Galactic midplane (with increasing $|Z|$) to be separated.

Figure 4 shows the theoretical isochrones before the stage of a clump giant (highlighted by the large symbols) for stars with metallicities $Z = 0.008$ (black squares and solid curve), $Z = 0.004$ (grey diamonds and solid curve), and $Z = 0.0004$ (black circles and dashed line) on the (a) $(H - W2) - M_{Ks}$ and (b) $(Ks - W2) - M_{Ks}$ diagrams according to the Padova database. It can be seen that almost all of the main-sequence, RGB, and clump giant stars fall into the narrow range of colors

$$0.03^m < (H - W2) < 0.1^m, -0.08^m < (Ks - W2) < 0.04^m. \quad (3)$$

The red dwarfs and RGB-tip giants turn out to be outside this range. Thus, applying these limitations by taking into account the possible reddening of stars, along with the criterion (2), we free the sample of clump giants from the main admixtures.

However, even before the rejection of stars, the narrow range of $(H - W2)$ and its independence of metallicity allow the reddening near the Sun and the influence of the admixtures of red dwarfs and RGB-tip giants to be estimated. Figures 5a and 5b show the $Ks - (H - W2)$ diagrams for all stars (not only the clump giants) in the regions with a radius of 8° around the Galactic north and south poles, respectively. The curves indicate the results of our moving averaging of the data over 15 points. It can be seen that the mean $\overline{(H - W2)}$ both southward and northward of the Sun has a minimum near $Ks \approx 7.8^m$. Judging by Fig. 4a, the decrease in $\overline{(H - W2)}$ at $6^m < Ks < 7.8^m$ implies a decrease in the fraction of RGB stars in the sample.

It can be seen that the minimum $\overline{(H - W2)}$ are 0.08^m and 0.10^m northward and southward of the Sun, respectively. The dereddened color at $0.005 < \mathbf{Z} < 0.015$ for most of the main sequence and the clump giants is $(H - W2)_0 = 0.052^m$. Then, $E_{(H-W2)} = 0.028^m$ and 0.048^m toward the north and south poles, respectively, at heliocentric distances of several hundred pc, behind most of the equatorial absorbing layer. Thus, the reddening/extinction to the south of the Sun is larger than that to the north. According to the most commonly used estimates of the extinction law, for example, from Cardelli et al. (1989), Draine (2003), and Indebetouw et al. (2005), $E_{(J-Ks)} \approx E_{(H-W2)}$, $E_{(B-V)} \approx 2E_{(H-W2)}$ and $A_V \approx 6.2E_{(H-W2)}$. The reddening estimates toward the poles obtained here are then in good agreement with those from Gontcharov (2010), $E_{(J-Ks)} = 0.02^m$ and 0.03^m , to the north and the south obtained when constructing the three-dimensional reddening map within 1.6 kpc of the Sun and with the estimates from Gontcharov (2012b), $E_{(B-V)} = 0.06^m$ and $A_V = 0.2^m$, toward the Galactic poles obtained by comparing the reddening/extinction maps from Gontcharov (2010), Schlegel et al. (1998), and Jones et al. (2011).

Taking into account the limitations (3), the estimates $E_{(Ks-W2)} = 0.62E_{(H-W2)}$ and $E_{(Ks-W1)} = 0.56E_{(H-W2)}$ according to the mentioned extinction laws, the possible reddening of the colors for stars farther than 700 pc, the photometric errors, and the change in dereddened colors due to the decrease in metallicity, we adopt the limitations $0 < (H - W2) < 0.25$, $-0.1 < (Ks - W2) < 0.16$, and $-0.04 < (Ks - W1) < 0.18$ in addition to the limitation (2) and $Ks < 11^m$ in order to select the clump giants. The final sample contains 76 801 and 71 624 clump giants with $b < -50^\circ$ and $b > 50^\circ$, respectively. It is the stars from this sample that are marked in Fig. 2 by the larger signs.

It can be seen from Fig. 4b that the change in $(Ks - W2)$ is a good indicator of the changes in metallicity. Figures 5c and 5d show the $Ks - (Ks - W2)$ diagrams for stars in the regions with a radius of 8° around the Galactic north (a) and south (b) poles for $Ks < 13^m$. To exclude most of the main sequence, we introduced the limitation $(Ks - W2) < 0.16^m$. The curves indicate the results of our moving averaging of the data over 55 points. It can be seen that the mean $\overline{(Ks - W2)}$ changes with distance, reflecting the change in mean metallicity from $\mathbf{Z} = 0.008 \pm 0.002$ to $\mathbf{Z} = 0.005 \pm 0.001$ according to the isochrones corrected for reddening $E_{(Ks-W2)} \approx 0.015^m$ as the height $|Z|$ changes from 0.6 to 3 kpc. It can be seen that the monotonic decrease in metallicity continues up to $(Ks - W2) \approx 0.025^m$ at $Ks = 12.5^m$,

i.e., to $\mathbf{Z} = 0.002$ at $|Z| = 6.4$ kpc. All of these metallicities are determined by this method very reliably and roughly correspond to the universally accepted values for these heights.

Next, we considered 18 sky fields: two with a radius of 8° around the Galactic poles and the symmetric sectors in the northern and southern hemispheres $66^\circ < |b| < 78^\circ$, $-20^\circ < l < 20^\circ$, $66^\circ < |b| < 78^\circ$, $70^\circ < l < 110^\circ$, $66^\circ < |b| < 78^\circ$, $160^\circ < l < 200^\circ$, $66^\circ < |b| < 78^\circ$, $250^\circ < l < 290^\circ$, $53^\circ < |b| < 61^\circ$, $-15^\circ < l < 15^\circ$, $53^\circ < |b| < 61^\circ$, $75^\circ < l < 105^\circ$, $53^\circ < |b| < 61^\circ$, $165^\circ < l < 195^\circ$, $53^\circ < |b| < 61^\circ$, $255^\circ < l < 285^\circ$.

In each field we performed a moving calculation of $E_{(H-W1)}/E_{(H-Ks)}$, $E_{(H-W2)}/E_{(H-Ks)}$, $E_{(H-W3)}/E_{(H-Ks)}$, $E_{(H-W4)}/E_{(H-Ks)}$ (it contains no useful information due to the low accuracy of the data), and other coefficients as a function of r with an averaging windows of 200 stars. The stars are arranged by r and the mean \bar{r} , along with the sought-for coefficients, is calculated for 200 stars with minimum r ; the star with minimum r is then excluded from the set of stars under consideration, a previously unused star with minimum r is then introduced instead of it, and the calculations of \bar{r} and the sought-for coefficients are repeated. As a result, we obtain several thousand solutions including \bar{r} with the corresponding set of sought-for coefficients for each sky field under consideration.

Among all of the analyzed coefficients, below we consider $E_{(H-W1)}/E_{(H-Ks)}$, $E_{(H-W2)}/E_{(H-Ks)}$, $E_{(H-W3)}/E_{(H-Ks)}$, because their variations can be directly compared with the results from Zasowski et al. (2009) and Gontcharov (2013). This analysis is not an exhaustive use of the available IR photometry at high latitudes. Other characteristics of stars and the medium can also be estimated from the same data.

RESULTS

Figure 6 shows the variations of $E_{(H-W2)}/E_{(H-Ks)}$ with heliocentric distance for the region with a radius of 8° around the Galactic north (a) and south (b) poles (black curves with grey error bands). Smaller values of the coefficient correspond to larger dust grain sizes and a larger extinction with a longer wavelength.

The dashes indicate the presumed variation of the coefficient within 500 pc of the Sun if the dust grain size distribution in the range 2 – 11 microns continues the trends of the distribution in the range 0.5 – 2 microns: at $r = 0$

the dashes indicate $E_{(H-W2)}/E_{(H-Ks)} = 1.7$ found by Gontcharov (2013), on average, for the solar neighborhood, while the variations indicated by the dashes correspond to the R_V variations shown in Fig. 1.

First of all, it can be seen from the figure that the coefficient under consideration outside the disk (i.e., at $|Z| > 0.1$ kpc) is everywhere smaller than that in the disk. Consequently, as was assumed by Gontcharov (2013), the fraction of fine dust in the disk is maximal, while the mean grain size is minimal. It can be seen that the mean dust grain size outside the disk decreases with increasing heliocentric distance and stabilizes or may begin to increase again farther than 2.4 kpc.

Figure 6c shows the results for the poles together. It can be seen that the values of $E_{(H-W2)}/E_{(H-Ks)}$ southward and northward of the Sun are very close at some distances, forming “nodes” to which the distance $r = 0$ also refers. These nodes are spaced, on average, 656 pc apart (the accuracy is discussed below) and are indicated by the vertical arrows at the bottom. The variations of the coefficient at the remaining distances anticorrelate, i.e., the decrease in coefficient to the south corresponds to its increase to the north and vice versa. The most prominent differences between the curves are highlighted in Fig. 6c as the shaded regions between them. The results for R_V indicated by the dashes show the same effect, although this study of R_V has little in common with that by Gontcharov (2012a): we considered different classes of stars – clump giants instead of RGB and OB stars (no common star), photometry in the H , Ks , and $W2$ bands instead of B_T , V_T , Ks (one common band from 2MASS). Other coefficients, without the Ks band, that are not shown here, for example, $E_{(H-W2)}/E_{(J-H)}$ and $E_{(H-W2)}/E_{(H-W1)}$, exhibit the same anticorrelation to the south and the north. Consequently, this effect cannot be attributed to the systematic photometric errors.

To estimate the accuracy of our results, we varied the averaging window in the range from 100 to 300 stars. In comparison with the window of 200 stars, high-frequency (~ 10 pc) variations of the coefficients under consideration manifest themselves for the window of 100 stars, which are unlikely to be real, while the amplitude of the long-period variations shown in Fig. 6 decreases noticeably for the window of 300 stars. However, these long-period variations are observed for any window considered and, moreover, their phase and period remain within ± 20 pc irrespective of the window size. Thus, it can be concluded that the nodes are spaced, on average, 656 ± 20 pc apart. This suggests that the variations are real, which is quite expectable, given that, as has been pointed out above, the relative accuracy of individual r

determined by the scatter of individual M_{Ks} is 15%. The formal relative accuracy of \bar{r} is then 1%, i.e., at least 30 pc. Of course, several systematic effects affecting the result were not taken into account and cannot be taken into account here. For example, the sample composition can change with distance from the Galactic midplane. However, we can hope for a smooth pattern of these systematic effects depending on coordinate Z . Then, the phase, step, and constancy of the period may not be determined quite correctly in the detected variations of the coefficients under consideration along Z , but the very fact of the existence of periodic or, more precisely, cyclic variations in the coefficients under consideration has been established firmly.

We also find a similar anticorrelation between the variations for the coefficients $E_{(H-W1)}/E_{(H-Ks)}$ and $E_{(H-W3)}/E_{(H-Ks)}$, which are shown for the same sky regions in Fig. 7. The presumed variations of the coefficients within 500 pc of the Sun based on the results from Gontcharov (2012a) and $E_{(H-W1)}/E_{(H-Ks)} = 1.5$ and $E_{(H-W3)}/E_{(H-Ks)} = 2$ from Gontcharov (2013) for $r = 0$ are also indicated here by the dashes. Just as from $E_{(H-W2)}/E_{(H-Ks)}$, it can be seen from these coefficients that the dust grains outside the disk are, on average, larger than those in the disk.

The errors of our results are represented by the individual vertical bars. The vertical straight lines indicate the distances marked by the arrows in Fig. 6. It can be seen that the nodes of variations for $E_{(H-W1)}/E_{(H-Ks)}$ coincide with those for $E_{(H-W2)}/E_{(H-Ks)}$, while the analogous results for $E_{(H-W3)}/E_{(H-Ks)}$ are barely seen because of the large photometric error in the $W3$ band.

Figure 8 shows the variations of $E_{(H-W2)}/E_{(H-Ks)}$ with heliocentric distance for symmetry sectors of the sky in the northern (black curves) and southern (grey curves) hemispheres: (a) $66^\circ < |b| < 78^\circ$, $-20^\circ < l < 20^\circ$, (b) $66^\circ < |b| < 78^\circ$, $70^\circ < l < 110^\circ$, (c) $66^\circ < |b| < 78^\circ$, $160^\circ < l < 200^\circ$, (d) $66^\circ < |b| < 78^\circ$, $250^\circ < l < 290^\circ$, (e) $53^\circ < |b| < 61^\circ$, $-15^\circ < l < 15^\circ$, (f) $53^\circ < |b| < 61^\circ$, $75^\circ < l < 105^\circ$, (g) $53^\circ < |b| < 61^\circ$, $165^\circ < l < 195^\circ$, (h) $53^\circ < |b| < 61^\circ$, $255^\circ < l < 285^\circ$. The same effects as those for the poles are seen: the results for the hemispheres are similar, anticorrelate between themselves, the dust outside the disk is everywhere coarser than that in the disk. However, these effects are less pronounced than those for the poles due to the influence of the errors in the photometric distances derived from Eq. (1). The maxima and minima of the coefficient variations in Fig. 8 are shifted along r relative to those in Fig. 6 approximately with the coefficient $(\sin b)^{-1}$. Consequently, the coarse and fine dust at high latitudes

is located in layers that alternate along $|Z|$ and are approximately parallel to the Galactic plane. This also explains the variations of $E_{(H-W2)}/E_{(H-Ks)}$ with latitude visible in the figure: at $53^\circ < |b| < 61^\circ$ it is, on average, smaller than that at $66^\circ < |b| < 78^\circ$. It can also be seen from the figure that there are no variations of the coefficient with longitude everywhere at high latitudes. Therefore, although here we considered only individual fields of the celestial sphere, our results undoubtedly refer to all high latitudes. However, as the size of the fields increases, the detected variations of the coefficients under consideration become invisible due to the errors of the photometric distances.

The detected consistency of the variations in the characteristics of the interstellar medium southward and northward of the Sun within at $-2.5 < Z < 2.5$ kpc, i.e., 5 kpc, is an unexpected result that requires a further confirmation. It is important that it could not be obtained before the appearance of WISE results, the first (in the history of astronomy) accurate IR photometry at high latitudes. This result suggests the connections between widely separated regions of the seemingly very tenuous interstellar medium, a unified large-scale structure of the medium within at least 5 kpc. This structure may have emerged long ago during the formation of our Galaxy and has been maintained for billions of years.

It may worth considering this structure as an alternation of layers of not fine and coarse dust but sorted and unsorted dust. The cause of the sorting is apparently the same as that in the spiral pattern of the disk the density wave and the corresponding periodic star formation. Based on the theory and observations, Fridman and Khoperskov (2011) showed that the motions of the Galactic medium along Z together with the motions along the Galactic plane constitute a unified three-component velocity vector field in the spiral density wave. It then worth noting that the structure we found here has a spatial step of $656 \times 2 = 1312$ pc, a value close to the typical distance between the Galactic spiral arms.

The anticorrelation in the arrangement of dust layers with different properties in the southern and northern hemispheres may be considered as a possible result of the periodic alternation of star formation due to a sharp increase in the density of the protogalactic medium alternately in the southern and northern hemispheres. This, in turn, can be explained by the tidal effect from a protogalaxy high-latitude satellite.

CONCLUSIONS

This study showed the possibility of jointly using accurate near- and mid-IR photometry from the 2MASS and WISE catalogues, respectively, to analyze the variations of the extinction law and the corresponding interstellar dust properties at high Galactic latitudes.

Owing to the high accuracy of the data, the large number of stars considered, and the convenience of using multicolor IR photometry, the modified method of extrapolation of the extinction law applied to clump giants turned out to be efficient for separating the spatial variations of the sample composition, metallicity, reddening, and properties of the medium. As a result, we found effects whose detection was not possible before the appearance of the 2MASS and WISE catalogues.

We analyzed the variations of the coefficients $E_{(H-W1)}/E_{(H-Ks)}$, $E_{(H-W2)}/E_{(H-Ks)}$ and $E_{(H-W3)}/E_{(H-Ks)}$ in 18 fields at high latitudes ($|b| > 50^\circ$). The dependence of our results on Galactic latitude and longitude is insignificant, which allows the results to be assigned to high latitudes as a whole.

As a result, we showed that the ratio of shortwavelength extinction to long-wavelength one everywhere outside the Galactic disk (i.e., at $|Z| > 100$ pc) is smaller than that in the disk and, accordingly, the mean dust grain size is larger, while the grain size distribution is shifted toward coarse dust. Specifically, the mean grain size initially increases sharply with $|Z|$, then decreases gradually, approaching a value typical of the disk at $|Z| \approx 2.4$ kpc, and, further out, stabilizes or may increase again.

The coefficients under consideration change with coordinate Z with a period of about 1312 ± 40 pc, coinciding every 656 ± 20 pc to the south and the north and showing a significant anticorrelation between their values in the southern and northern hemispheres at intermediate Z . A unified large-scale periodic structure of the interstellar medium at high latitudes within at least 5 kpc manifests itself in this way. These periodic variations were also found in the three-dimensional map of variations in extinction coefficient R_V constructed by Gontcharov (2012a) through the reduction of different photometric data for stars of different classes.

The detected structure of the medium outside the Galactic disk is assumed to be maintained by a density wave just as the spiral structure of the disk.

ACKNOWLEDGMENTS

In this study, we used results from the Two Micron All Sky Survey (2MASS) and Wide-field Infrared Survey Explorer (WISE) as well as resources from the Strasbourg Astronomical Data Center (Centre de Données astronomiques de Strasbourg). This study was supported by Program P21 of the Presidium of the Russian Academy of Sciences and the Ministry of Education and Science of the Russian Federation under contract 8417.

References

1. N.G. Bochkarev, *Fundamentals of the Physics of Interstellar Medium* (LIBROKOM, Moscow, 2010), p. 298 [in Russian].
2. A. Bressan, P. Marigo, L. Girardi, et al.), *Mon. Not. R. Astron. Soc.* **427**, 127 (2012).
3. J.A. Cardelli, G.C. Clayton and J.S. Mathis, *Astrophys. J.* **345**, 245 (1989).
4. B.T. Draine, *Ann. Rev. Astron. Astrophys.* **41**, 241 (2003).
5. ESA, *Hipparcos and Tycho catalogues* (ESA, 1997).
6. A.M. Fridman and A.V. Khoperskov, *Physics of Galactic Disks* (Fizmatlit, Moscow, 2011; Cambridge International Science, 2012), pp. 385-387.
7. G.A. Gontcharov, *Astron. Lett.* **34**, 785 (2008).
8. G.A. Gontcharov, *Astron. Lett.* **36**, 584 (2010).
9. G.A. Gontcharov, *Astron. Lett.* **38**, 12 (2012a).
10. G.A. Gontcharov, *Astron. Lett.* **38**, 87 (2012b).
11. G.A. Gontcharov, *Astron. Lett.* **39**, 83 (2013).
12. E. Høg, C. Fabricius, V.V. Makarov, et al., *Astron. Astrophys.* **355**, L27 (2000).

13. R. Indebetouw, J.S. Mathis, B.L. Babler, et al., *Astrophys. J.* **619**, 931 (2005).
14. D.O. Jones, A.A. West, J.B. Foster, *Astron. J.* **142**, 44, (2011).
15. F. van Leeuwen, *Astron. Astrophys.* **474**, 653 (2007).
16. M. Lopez-Corredoira, A. Cabrera-Lavers, F. Garzon, et al., *Astron. Astrophys.* **394**, 883 (2002).
17. S.R. Majewski, G. Zasowski and D.L. Nidever, *Astrophys. J.* **739**, 25 (2011).
18. P. Marigo, L. Girardi, A. Bressan, et al., *Astron. Astrophys.* **482**, 883 (2008).
19. D.J. Schlegel, D.P. Finkbeiner, M. Davis, *Astrophys. J.* **500**, 525, (1998).
20. M.F. Skrutskie, R.M. Cutri, R. Stiening, et al., *Astron. J.* **131**, 1163 (2006); <http://www.ipac.caltech.edu/2mass/releases/allsky/index.html>.
21. V. Strizys, *Multicolor Stellar Photometry* (Pachart, Tucson, 1992; Mokslas, Vilnyus, 1977).
22. E.L. Wright, P.R.M. Eisenhardt, A.K. Mainzer et. al., *Astron. J.* **140**, 1868 (2010); <http://irsa.ipac.caltech.edu/Missions/wise.html>
23. G. Zasowski, S.R. Majewski, R. Indebetouw, et al., *Astrophys. J.* **707**, 510 (2009).

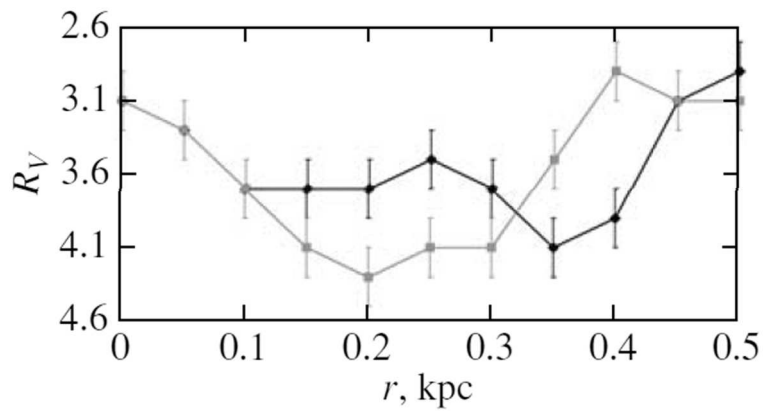


Figure 1: Coefficient R_V versus heliocentric distance for the region with a radius of 8° around the Galactic north (black diamonds, curve, and vertical error bars) and south (grey squares, curve, and vertical error bars) poles.

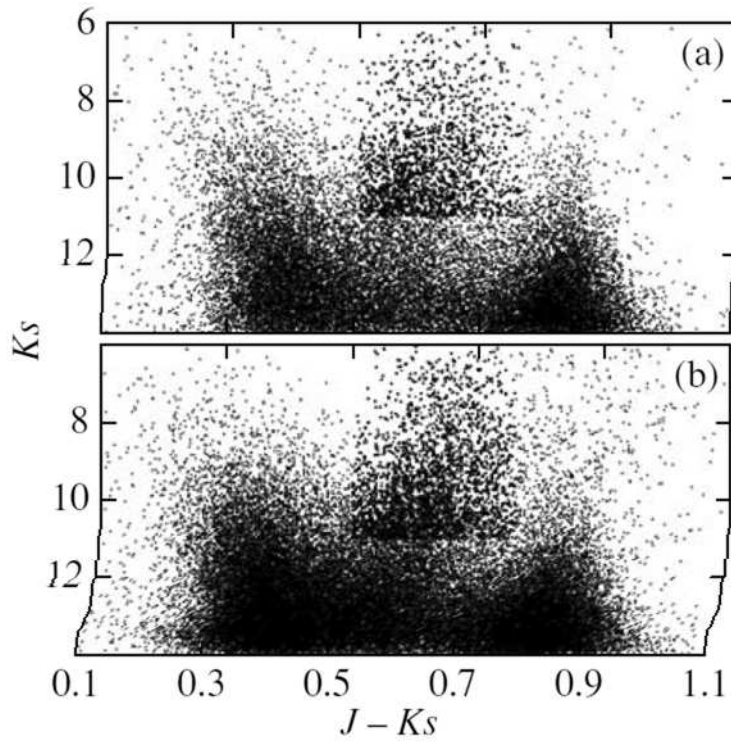


Figure 2: Distribution of the stars under consideration on the $(J - K_s) - K_s$ diagram (a) in the sky region with a radius of 8° around the Galactic north pole and (b) in the sky sector $-15^\circ < l < 15^\circ$, $-61^\circ < b < -53^\circ$. The selected stars are marked by the larger signs in the upper parts of the graphs.

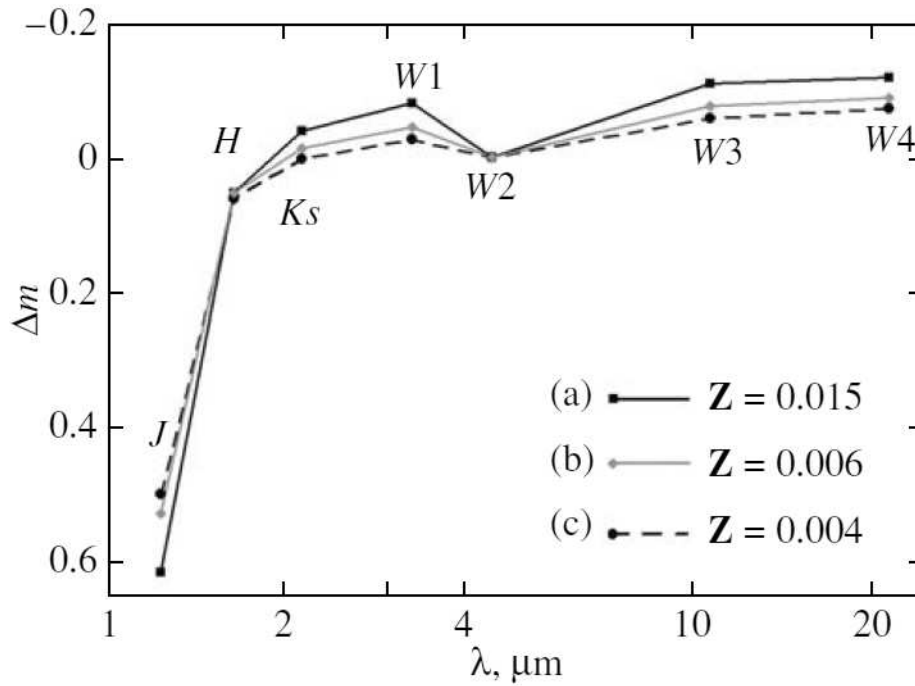


Figure 3: Theoretical spectral energy distribution for a typical clump giant with an age of 10×10^9 yr for metallicities (a) $Z = 0.015$ (black squares and solid curve), (b) $Z = 0.006$ (grey diamonds and solid curve), and (c) $Z = 0.004$ (black circles and dashed line) in the (from left to right) J , H , Ks , $W1$, $W2$, $W3$, and $W4$ bands expressed in magnitudes relative to the $W2$ magnitude.

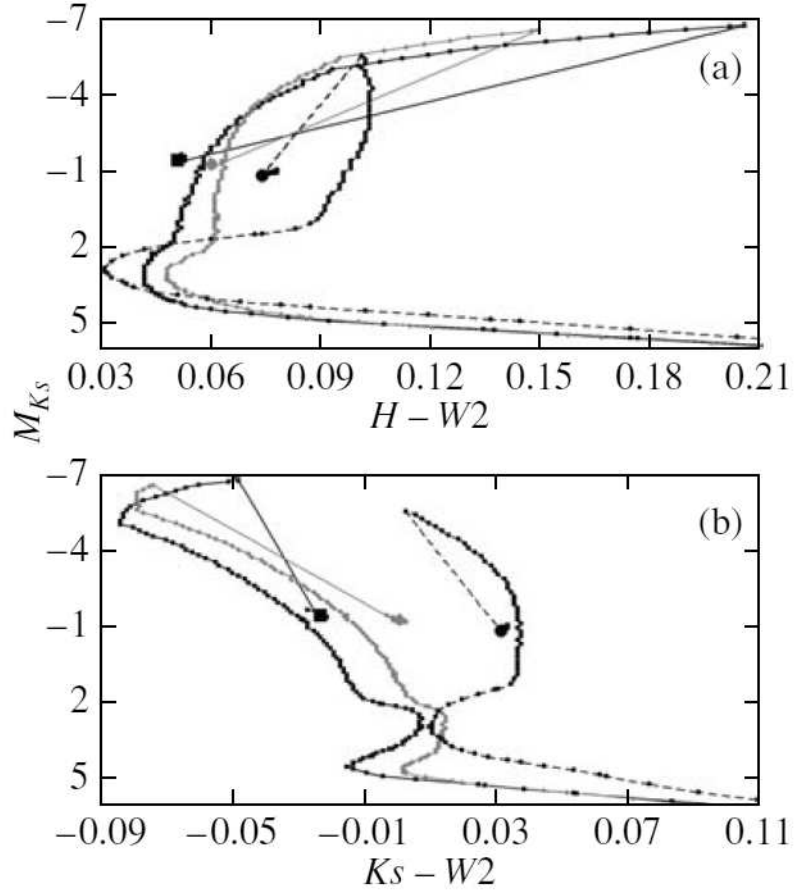


Figure 4: Theoretical isochrones before the stage of a clump giant (highlighted by the large symbols) for stars with metallicities $Z = 0.008$ (black squares and solid curve), $Z = 0.004$ (grey diamonds and solid curve, and $Z = 0.0004$ (black circles and dashed line) on the (a) $(H - W2) - M_{K_s}$ and (b) $(K_s - W2) - M_{K_s}$ diagrams according to the Padova database (<http://stev.oapd.inaf.it/cmd>; Marigo et al. 2008; Bressan et al. 2012).

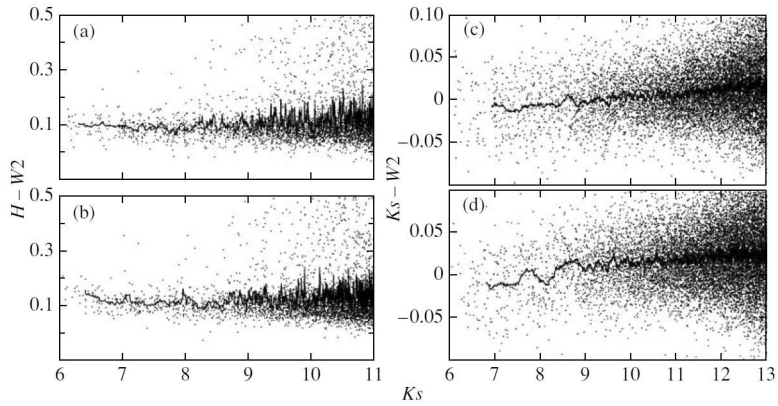


Figure 5: $Ks - (H - W2)$ and $Ks - (Ks - W2)$ diagrams for stars in the regions with a radius of 8° around the Galactic north ((a) and (c)) and south ((b) and (d)) poles. Only the stars with $(Ks - W2) < 0.16^m$ were left on the $Ks - (Ks - W2)$ diagram. The curves indicate the results of our moving averaging of the data over 15 and 55 points for $(H - W2)$ and $(Ks - W2)$, respectively.

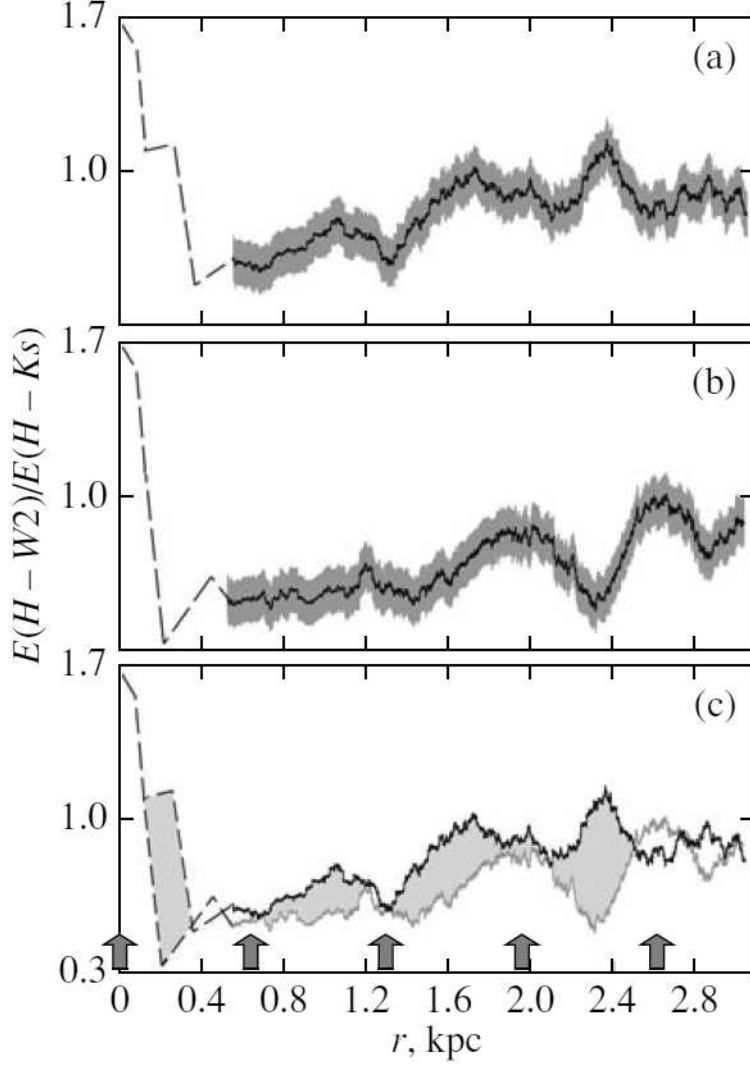


Figure 6: $E_{(H-W2)}/E_{(H-Ks)}$ versus heliocentric distance for the region with a radius of 8° around the Galactic north (a) and south (b) poles (black curves with grey error bands). The dashes indicate the presumed variation of the coefficient within 500 pc of the Sun; (c) combined results for the poles: the most prominent differences between the curves are highlighted as the shaded regions between the plots; the arrows indicate the distances at which the results for the poles are similar.

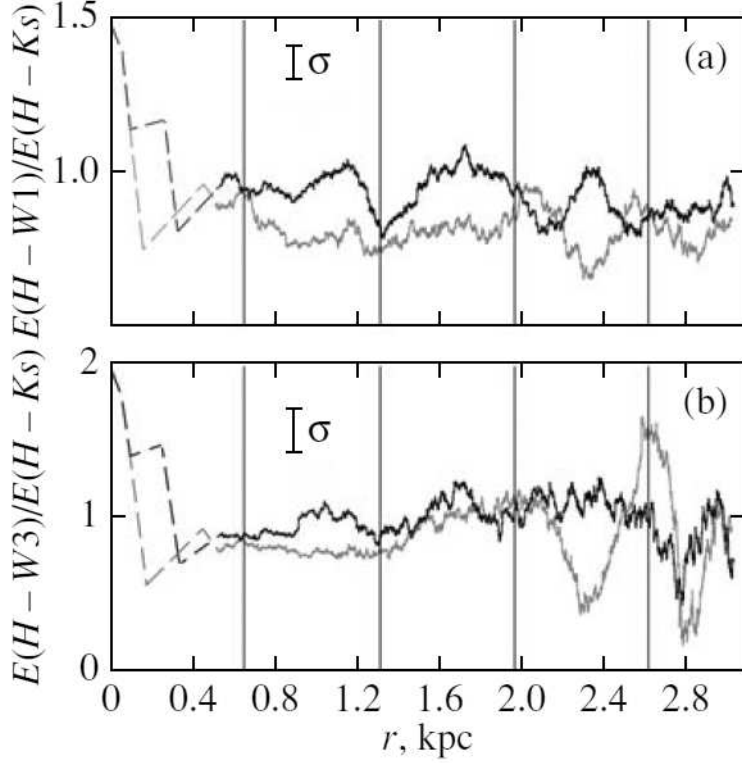


Figure 7: $E_{(H-W1)}/E_{(H-Ks)}$ (a) and $E_{(H-W3)}/E_{(H-Ks)}$ (b) versus heliocentric distance for the region with a radius of 8° around the Galactic north (black curves) and south (grey curves) poles. The dashes indicate the presumed variations of the coefficients within 500 pc of the Sun. The errors are represented by the individual vertical bars. The vertical straight lines indicate the distances marked by the arrows in Fig. 6.

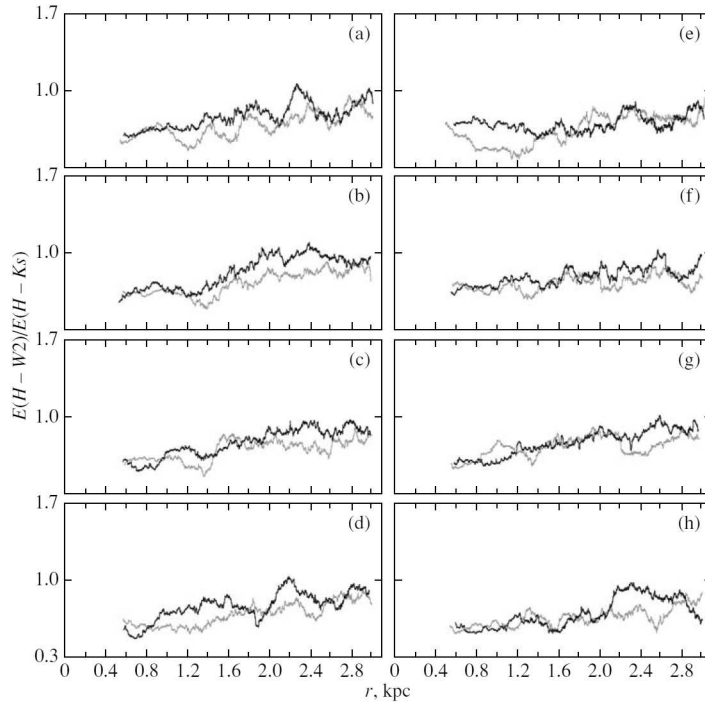


Figure 8: $E_{(H-W2)}/E_{(H-Ks)}$ versus heliocentric distance for symmetric sectors of the sky in the northern (black curves) and southern (grey curves) hemispheres: (a) $66^\circ < |b| < 78^\circ$, $-20^\circ < l < 20^\circ$, (b) $66^\circ < |b| < 78^\circ$, $70^\circ < l < 110^\circ$, (c) $66^\circ < |b| < 78^\circ$, $160^\circ < l < 200^\circ$, (d) $66^\circ < |b| < 78^\circ$, $250^\circ < l < 290^\circ$, (e) $53^\circ < |b| < 61^\circ$, $-15^\circ < l < 15^\circ$, (f) $53^\circ < |b| < 61^\circ$, $75^\circ < l < 105^\circ$, (g) $53^\circ < |b| < 61^\circ$, $165^\circ < l < 195^\circ$, (h) $53^\circ < |b| < 61^\circ$, $255^\circ < l < 285^\circ$.